








Asteroseismology of a Double-mode High-amplitude δ Scuti Star TIC 448892817

Chenglong Lv^{1,2} , Ali Esamdin^{1,2} , J. Pascual-Granado³ , A. García Hernández⁴ , and A. Hasanzadeh⁵ ¹ Xinjiang Astronomical Observatory, Chinese Academy of Sciences, Urumqi, Xinjiang 830011, People's Republic of China; aliyi@xao.ac.cn² School of Astronomy and Space Science, University of Chinese Academy of Sciences, Beijing 100049, People's Republic of China³ Instituto de Astrofísica de Andalucía—CSIC, E-18008 Granada, Spain⁴ Universidad de Granada, Dept. Theoretical Physics and Cosmology, E-18071, Granada, Spain⁵ Institute of Geophysics, University of Tehran, Tehran, Iran

Received 2022 June 13; revised 2022 September 6; accepted 2022 September 21; published 2022 October 26

Abstract

We propose that TIC 448892817 is a double-mode high-amplitude δ Scuti star. The radial modes detected in this star provide a unique opportunity to exploit asteroseismic techniques up to their limits. 30 significant frequencies are detected by frequency analysis, while two of them are independent frequencies, i.e., $F_0 = 13.43538(2) \text{ day}^{-1}$ and $F_1 = 17.27007(4) \text{ day}^{-1}$. The ratio of f_1/f_2 is measured to be $0.777957(2)$, suggesting that this target is a double-mode δ Scuti star. Nearly all the light variation is due to these two modes and their combination frequencies, but several other frequencies of very low amplitude are also present. The stellar evolutionary models were constructed with different mass M and metallicity Z using Modules for Experiments in Stellar Astrophysics (MESA). The frequency ratio f_1/f_2 obtained by the model is smaller than those obtained by observation. This might be caused by the rotation of the star pointing that rotational effects are more important than previously thought in HADS stars. This is something that deserves to be investigated in future works with models including rotational effects for moderate to intermediate rotators such as FILOU. On the other hand, the parameters obtained from MESA agree well with previous results as well as by observational spectra. The best-fitting model shows that TIC 448892817 is close to entering the first turnoff of the main sequence. In order to accurately determine the effective temperature and metallicities, thus further narrowing the parameter space of this star, we suggest high-resolution spectra is highly desired in the future.

Unified Astronomy Thesaurus concepts: [Asteroseismology \(73\)](#); [Delta Scuti variable stars \(370\)](#); [Stellar oscillations \(1617\)](#)

1. Introduction

A useful task for diagnosing the physical structure of pulsating stars is asteroseismology (e.g., Brown & Gilliland 1994; Dupret et al. 2004; Aerts et al. 2010; Catelan & Smith 2015; García & Ballot 2019; Daszyńska-Daszkiewicz et al. 2020). During the last years, as a number of missions have received high-resolution data (such as the Microvariability and Oscillations of STars; Walker et al. 2003; Convection, Rotation, and planetary Transits; Auvergne et al. 2009; and Kepler; e.g., Gilliland et al. 2010; Koch et al. 2010), so asteroseismology have been extensively studied (e.g., Yu et al. 2018; Aerts 2021; Bowman et al. 2021; Mombarg et al. 2021; Stello et al. 2022). More recently, TESS surveys most ($\sim 85\%$) of the sky within the 26 sectors during two years of the primary mission (Ricker et al. 2015) and contributed high-quality photometric light curves of nearby stars (e.g., Campante et al. 2016; Huber et al. 2019). Using such a high-quality database for research will make a significant contribution to the development of asteroseismology as well as stellar structure and evolution.

The δ Scuti star overlay in the Hertzsprung–Russell diagram is roughly divided into two parameter space types, one for the transition region from slowly rotating low-mass stars with radiative cores and thick convective envelopes ($M \leq 1.5 M_\odot$), and the other for rapidly rotating intermediate mass stars with

convective cores and predominantly radiative envelopes ($M \geq 2.5 M_\odot$). Such variations in the structure of stars allow the exploration of many different aspects of physics, including pulsation, rotation, magnetic fields, and chemical peculiarities (e.g., Murphy et al. 2015; Saio et al. 2015; Chen et al. 2019; Bowman et al. 2021; Thomson-Paressant et al. 2021). Therefore, the investigation of δ Scuti stars is extremely important for testing stellar evolution models. Many pulsation frequencies can be detected in δ Scuti stars corresponding to different pulsation modes. These are mainly radial and nonradial modes (e.g., Breger 2000; Uytterhoeven et al. 2011) and are typically excited by the κ mechanism (e.g., Breger 2000; Aerts et al. 2010). These pulsation modes are generally identified as low-radial-order (n) low-degree (l) pressure (p) modes (e.g., Viskum et al. 1998; Aerts et al. 2010; Uytterhoeven et al. 2011; Chen et al. 2019). The δ Scuti stars also exist in binary systems (e.g., Chen et al. 2019; Lv et al. 2021), and more precise stellar parameters are obtained by comparing the results of the binary orbital parameters with the results of the asteroseismology analysis. Thus, these targets are excellent samples for asteroseismic study, as they could improve our understanding of stellar structure and evolution (e.g., Guo et al. 2019; Murphy et al. 2020; Miszuda et al. 2021).

High-amplitude δ Scuti (HADS) stars are a subclass of δ Scuti stars, which are typically slow rotators with $v \sin i < 30 \text{ km s}^{-1}$, pulsation periods between 1 and 6 hr, and peak-to-peak light amplitudes above 0.3 mag (McNamara 2000). Prior to the release of high-precision space data, the detected HADS usually had only one or two radial pulsation modes of the fundamental and/or first overtone mode (e.g., Poretti et al. 2005;



Original content from this work may be used under the terms of the [Creative Commons Attribution 4.0 licence](#). Any further distribution of this work must maintain attribution to the author(s) and the title of the work, journal citation and DOI.

Yang et al. 2012; Niu et al. 2017; Xue et al. 2018; Yang et al. 2018). Advances in sophisticated data processing techniques, such as Lares-Martiz et al. (2020), have made possible that frequencies of low amplitude could be found in the spectrum of HADS as well (e.g., Poretti et al. 2011; Bowman et al. 2021). According to the ratio among the frequencies, the radial modes of HADS could be identified (Petersen 1973), and then by constructing radial frequencies models and comparing the models ratio with the observed ratio, several basic parameters of the star could be obtained, as well as the evolutionary stage (e.g., Xue et al. 2018; Bowman et al. 2021; Daszyńska-Daszkiewicz et al. 2022; Lv et al. 2022). A detailed seismic modeling of SX Phe performed by Daszyńska-Daszkiewicz et al. (2020), confirmed its post-main-sequence evolutionary stage by using a high-precision photometry collected from TESS mission. Lv et al. (2021) report a detailed light curve analysis of the Kepler target KIC 12602250, and their results show that KIC 12602250 is just pulsating at two radial frequencies. It seems unusual for a low amplitude δ Scuti to have such a clean spectrum, it might be helpful to explore the difference between HADS and normal δ Scuti stars. Therefore, detecting low-amplitude frequencies will enrich the features of light variation and improve the understanding of HADS.

TIC 448892817 ($\alpha_{2000} = 14^{\text{h}}:26^{\text{m}}:05.899^{\text{s}}$, $\delta_{2000} = +01^{\circ}:26':25''.727$) was classified as a HADS with a pulsation period of 0.07443 days by Khruslov & Kusakin (2013). Recently, Hasanzadeh et al. (2021) conducted a statistical analysis of the relations between the asteroseismic indices and stellar parameters of δ Scuti stars, TIC 448892817 is included in the statistical work and the asteroseismic indices are given. Combining the pulsation characteristics of HADS one may presume that the mode of highest amplitude is a radial mode. Since there is no rotational splitting for radial modes, it provides a very valuable constraint on the models. One would also expect that other radial modes might be present, which can be identified from the period ratio in the Petersen diagram (Petersen 1973). The double radial modes and low-order regime (around F0) frequencies allow to analyze the stellar asteroseismic indices, making it an excellent target for study. In order to limit the parameters more accurately and attempt to give the evolutionary stages of this star, we downloaded the high-precision photometric data provided by TESS and conducted a detailed study. The fundamental parameters of this star are listed in Table 1.

In this paper, Section 2 introduces the observations of TIC 448892817. The frequency analysis is presented in Section 3. In Section 4, we construct stellar evolution models and make pulsation frequency fitting. A brief discussion and the conclusions are presented in Sections 5.

2. Observations and Data Reduction

The TESS Space Telescope (Ricker et al. 2015) observed TIC 448892817 during Sector 5 for 25.6 days from Barycentric Julian Date (BJD) 2458438.06485 to 2458463.70366 in 2 minutes cadence, and for 26 days from BJD 2458437.99541 to 2459463.99534 in 30 minutes cadence. All the data were downloaded from TESS Asteroseismic Science Operations Center (TASOC) database.⁶ Since the lengths of the two data sets are approximately equal, shorter exposures allow for larger Nyquist detection limits. Therefore, we only used 2 minute observations in the subsequent study.

Table 1
Basic Properties of TIC 448892817

Parameters	TIC 448892817	
T mag	12.2277	a
Period	0.07443 days	c
T_{eff}	7253 K	a
	7798 ± 200 K	b
$\log g$	3.956 dex	a
	4.004 ± 0.021 dex	b
Fe/H	-0.227	a
	-0.149 ± 0.011	b
B	12.28 mag	a
V	12.67 mag	a
J	11.87 mag	a
H	11.67 mag	a
K	11.67 mag	a
Gaia	12.48 mag	a

Note. (a) Parameters from the TASOC. (b) Parameters from the LAMOST. (c) (Khruslov & Kusakin 2013).

In this work we use the corrected flux and convert it to magnitude. The average value for each sector is then subtracted to obtain the corrected time series. After the above processing, a rectified light curve of 17246 data points with a time span of about 25.6 days was finally obtained. Figure 1 shows a portion of the rectified light curve of TIC 448892817 covering 2.9 days for the 2 minutes cadence, and the peak-to-peak amplitude of TIC 448892817 obtained from the rectified light curve is ~ 0.32 mag, which is typical for HADS stars.

3. Frequency Analysis

To analyze the pulsating behavior of TIC 448892817, the software PERIOD 04⁷ (Lenz & Breger 2005) was used during this work. A minimum sampling frequency is set for the Nyquist frequency to prevent alias frequencies (Bowman et al. 2016). The Nyquist frequency of 2 minute cadence observations is $f_N = 360 \text{ day}^{-1}$, well above our limit range of $0 < f < 50 \text{ day}^{-1}$ for the extracted frequencies. The range of frequencies we extracted covers the typical pulsation interval of δ Scuti stars. In order to distinguish between adjacent closer frequencies in the power spectrum, we use the resolution frequency $f_{\text{res}} = 1.5/\Delta T$ (Loumos & Deeming 1978), where ΔT is the length of the data set. When the difference between these two frequencies is larger than the resolution frequency, we assume that these two frequencies have been resolved. The resolution frequency $f_{\text{res}} = 1.5/\Delta T$ is 0.0586 day^{-1} for TESS Sector 5.

The rectified light curve was fitted with the following formula:

$$m = m_0 + \sum_{i=1}^N A_i \sin(2\pi(f_i t + \phi_i)), \quad (1)$$

where m_0 is the zero point, A_i is the amplitude, f_i is the frequency, and ϕ_i is the corresponding phase. In the process of extracting significant frequencies, we usually identify the highest peaks as significant frequencies. The multifrequency least-square fit of the light curve for all detected significant frequencies is then performed using Equation (1) to obtain solutions for all frequencies. The residuals are obtained by

⁶ TASOC: https://tasoc.dk/search_data/.

⁷ <https://www.univie.ac.at/tops/Period04/>

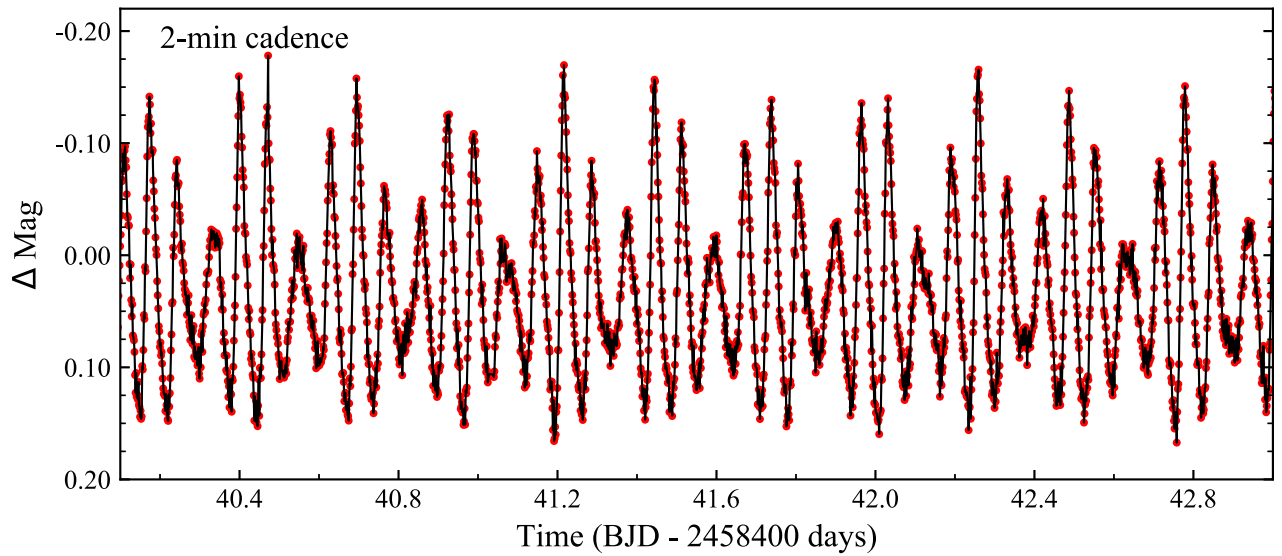


Figure 1. A portion of the rectified light curve of TIC 448892817 covering 2.9 days for the 2 minutes cadence. The amplitude of the light curve is about 0.32 mag.

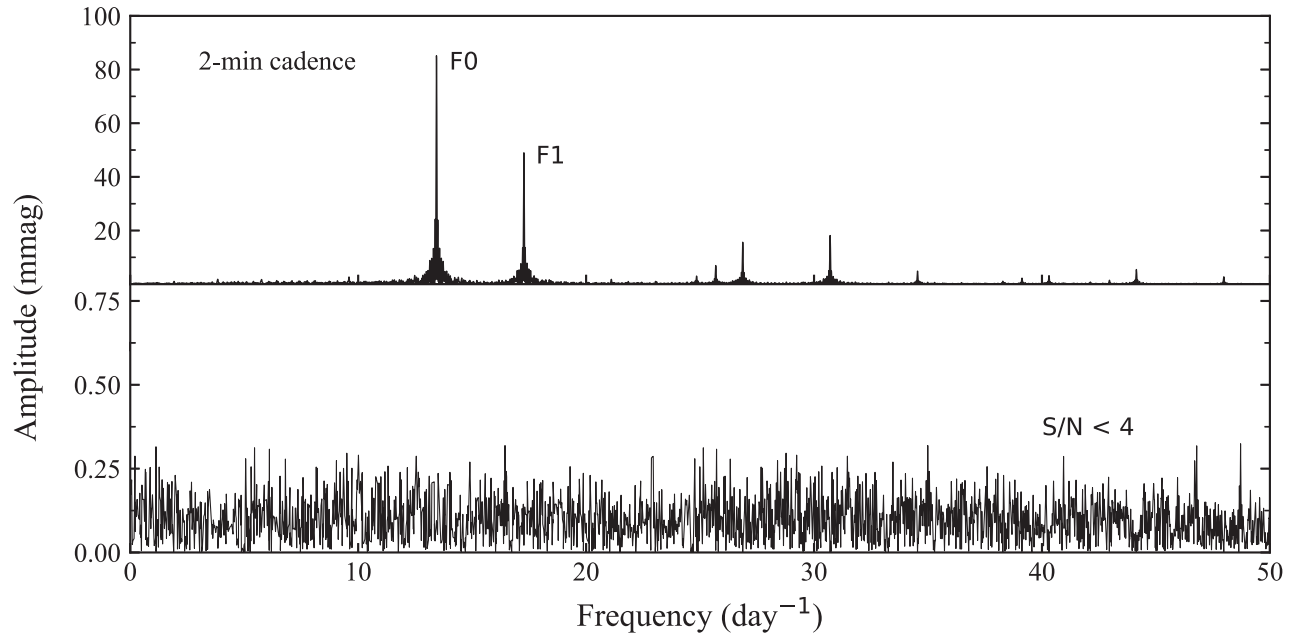


Figure 2. Fourier amplitude spectra for the light curve of TIC 448892817. The top panel shows the independent frequencies F0 and F1 of 2 minutes cadence. The bottom panel shows the residual spectrum after the extraction of all significant frequencies. No peak is statistically significant in the residual.

subtracting the theoretical light curve constructed by the above solution from the rectified data and continuing the next search using the obtained residuals, repeating the above steps until no significant peaks are found in the spectrum. After any new detection, the set of previously detected frequency values is refined. As the criterion for determining if a detected peak is significant or not we use the signal-to-noise ratio ($S/N > 4$) suggested by Breger et al. (1993). The frequency uncertainty was determined according to the method proposed by Montgomery & O’donoghue (1999). Figure 2 shows the amplitude spectra for 2 minute cadence data, and the bottom panel shows the residual amplitude spectra after all significant peaks were prewhitened.

Through Fourier transforming the spectrum of TIC 448892817, a total of 30 frequencies were detected.

Stellingwerf (1979) was one of the first papers to predict the period ratios based in theoretical structure models and presented the period ratios of the first two radial modes as: $f_1/f_2 = (0.756-787)$. The two high-amplitude modes of TIC 448892817 have a frequency ratio of 0.777957(2) identifying them as the fundamental and first overtone radial modes (Breger 2000). Combination frequencies were identified by searching for linear sum and difference frequencies, $n\nu_i \pm m\nu_j$, with the Loumos & Deeming (1978) criterion as a tolerance and assuming that the highest-amplitude peaks within a combination family are the real pulsation mode frequencies (Kurtz et al. 2015). Therefore, the fundamental frequency f_1 with “F0”, first overtone f_2 with “F1” and the combination frequencies (i.e., $f_3, f_5, f_8 \dots f_{13}$) and harmonics frequencies (i.e., f_4, f_6, f_7) of the two radial modes are listed in Table 2. Note that some peaks originated from combinations (e.g., F0+F1 and

Table 2
The Radial Pulsation Mode Frequencies in SC data of TIC 448892817

f_i	Frequency (day^{-1})	Amplitude (mmag)	Phase (rad)	S/N	Comment
1	13.43538 ± 0.00002	84.71 ± 0.09	0.8868 ± 0.0002	224.5	F0
2	17.27007 ± 0.00004	48.53 ± 0.09	0.3028 ± 0.0003	139.6	F1
3	30.7054 ± 0.0001	18.15 ± 0.09	0.1961 ± 0.0008	124.3	F0+F1
4	26.8706 ± 0.0001	15.59 ± 0.09	0.8888 ± 0.0009	89.6	2F0
5	44.1406 ± 0.0003	5.51 ± 0.09	0.143 ± 0.003	53.7	2F0+F1
6	34.5396 ± 0.0004	4.81 ± 0.09	0.341 ± 0.003	36.4	2F1
7	40.3057 ± 0.0006	3.14 ± 0.09	0.048 ± 0.004	26.4	3F0
8	47.9752 ± 0.0007	2.80 ± 0.09	0.759 ± 0.005	34.3	F0+2F1
9	9.5939 ± 0.0008	2.30 ± 0.09	0.498 ± 0.006	5.7	2F0-F1
10	21.1044 ± 0.0009	1.99 ± 0.09	0.439 ± 0.007	13.1	2F1-F0
11	3.836 ± 0.001	1.92 ± 0.09	0.315 ± 0.007	4.5	F1-F0
12	23.033 ± 0.002	0.94 ± 0.09	0.65 ± 0.02	6.9	3F0-F1
13	24.904 ± 0.002	0.98 ± 0.09	0.28 ± 0.01	6.6	3F1-2F0

Note. Among these frequencies, two peaks are independent frequencies, others are harmonic or combinations (denoted by f_i).

2F1) in the upper panel appear to correspond with aliases in the lower panel. Since this happens just with a few peaks and, taking into account that the observations are from different sectors, it appears it is just coincidentally. The remaining 17 frequencies are nonradial pulsation frequencies listed in Table 3. It is worth noting that $21.851(2) \text{ day}^{-1}$ is in F0/F2 range could be second overtone, we estimate the pulsation constant Q with the value of the stellar mean density (see Section 3.1) through the relation $P\sqrt{\bar{\rho}/\rho_{\odot}} = Q$, P is the period, the pulsation constant Q of $21.851(2) \text{ day}^{-1}$ is $0.0181(8)$. The pulsation constant is typically 0.020 for the second overtone of a δ Scuti star (Antonello & Pastori 1981), so the second overtone is excluded.

3.1. Studying the Large Separation

Despite the fact that δ Scuti stars do not pulsate in the asymptotic regime, there exists several works related to the search for large separations in their pulsation spectra since the end of the twentieth century (e.g., Handler & Breger 1997; Breger et al. 1999; García Hernández et al. 2009, 2013; Páparó et al. 2016; Bedding et al. 2020). The revolution came with the establishment of a relation between this large separation in the low-order regime and the stellar mean density, from the modeling (e.g., Reese et al. 2008; Suárez et al. 2014; Ouazzani et al. 2015) and, especially, from the observations (e.g., García Hernández et al. 2015; García Hernandez et al. 2017; Bedding et al. 2020; Hasanzadeh et al. 2021). It was demonstrated that this relation is invariant to rotation (e.g., Reese et al. 2008; García Hernández et al. 2015), although the value of $\Delta\nu$ itself does change from a nonrotating to a rotating star of the same mass.

To find the large separation, $\Delta\nu$, in the low-order regime of TIC 448892817, we followed the methodology of García Hernández et al. (2009, 2013) and Ramón-Ballesta et al. (2021), using the Fourier transform (FT), the autocorrelation function (AC), and the histogram of frequency differences (HFD). When doing all these transformations, the amplitudes of the frequencies have been equalled to one. We just selected the frequencies listed in Table 3 in order to avoid combination frequencies that do not correspond to excited modes. The result of this procedure is shown in left panel of Figure 3, where the black line is the FT, the blue line is the AC and the gray bars represent the HFD. All the transforms have been normalized to

Table 3
Additional Independent Frequencies Extracted from the 25.6 days 2 minutes Cadence TESS Data of TIC 448892817

f_{Si}	Frequency (day^{-1})	Amplitude (mmag)	Phase (rad)	S/N
1	25.6870 ± 0.0003	7.00 ± 0.09	0.830 ± 0.002	25.6
2	24.8466 ± 0.0006	3.05 ± 0.09	0.332 ± 0.005	19.2
3	39.1209 ± 0.0008	2.45 ± 0.09	0.832 ± 0.006	16.6
4	42.956 ± 0.001	1.65 ± 0.09	0.599 ± 0.008	12.6
5	38.282 ± 0.002	1.07 ± 0.09	0.34 ± 0.01	9.0
6	29.519 ± 0.002	0.82 ± 0.09	0.50 ± 0.02	6.5
7	42.121 ± 0.002	0.83 ± 0.09	0.55 ± 0.02	7.8
8	21.851 ± 0.002	0.79 ± 0.09	0.81 ± 0.02	6.1
9	26.131 ± 0.003	0.72 ± 0.09	0.38 ± 0.02	6.0
10	24.640 ± 0.003	0.71 ± 0.09	0.40 ± 0.02	5.7
11	33.259 ± 0.003	0.62 ± 0.09	0.95 ± 0.02	5.5
12	40.879 ± 0.003	0.58 ± 0.09	0.01 ± 0.02	5.9
13	35.287 ± 0.004	0.53 ± 0.09	0.77 ± 0.03	4.3
14	36.471 ± 0.004	0.50 ± 0.09	0.76 ± 0.03	4.3
15	38.374 ± 0.004	0.48 ± 0.09	0.61 ± 0.03	4.4
16	22.286 ± 0.004	0.47 ± 0.09	0.07 ± 0.03	4.4
17	33.138 ± 0.004	0.42 ± 0.09	0.08 ± 0.03	4.1

Note. F0, F1, and all their significant combinations and harmonics frequencies have been removed.

the highest peak for visualization reasons. As can be seen, a clear peak at around 3.8 day^{-1} ($44 \mu\text{Hz}$) appears in the AC and the bf HFD (buried under the red dotted-dashed line). This value is compatible with that found by Hasanzadeh et al. (2021). The FT does not show a peak around $\Delta\nu$ although it shows the half, around $22 \mu\text{Hz}$, but also $1/3$ ($14.5 \mu\text{Hz}$) and $1/4$ ($11 \mu\text{Hz}$). The absence of the of $\Delta\nu$ in the FT but its half is something expectable (see, for example, García Hernández et al. 2009) and the presence of more submultiples indicates that the correct value is 44 and not $22 \mu\text{Hz}$.

We can also take a look to the échelle diagram using this value. In right panel of Figure 3, we can clearly see how the ridges follow $\Delta\nu$. In this diagram, we have also added the fundamental mode and the first overtone to the nonradial modes used in the transformations. The frequencies plotted have amplitudes of 1, and those placed in the lowest part of the diagram correspond to F0 and F1. They are also separated by 3.8 day^{-1} despite they also show a ratio of $F0/F1 = 0.777957(2)$. This coincidence happened just by chance since F0 and F1 usually are not separated by $\Delta\nu$. The échelle diagram allows us

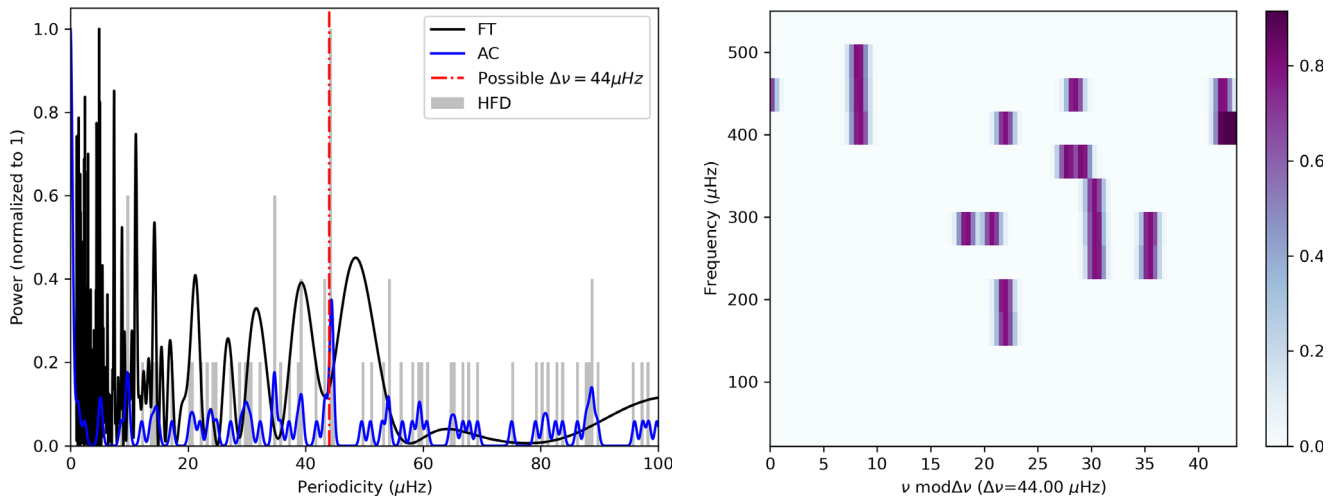


Figure 3. The left panel shows the procedure to find $\Delta\nu$. The black line represents the Fourier transform (FT) of the frequencies, the blue line is the autocorrelation function (AC), and the gray lines plot a histogram of frequency differences (HFD), following the methodology of García Hernández et al. (2009, 2013) and Ramón-Ballesta et al. (2021). The red dotted–dashed line indicates the identified value of $\Delta\nu = 3.8 \text{ day}^{-1}$ ($44 \mu\text{Hz}$), corresponding to the most prominent peak in the AC and HFD (see details in the text). The right panel shows an échelle diagram of the frequencies depicted with a normalized amplitude of 1 in purple. The value of 3.8 day^{-1} ($44 \mu\text{Hz}$) is used for the plot. The organization of the frequencies is clearly visible.

to constrain the uncertainty in $\Delta\nu = 3.80 \pm 0.01 \text{ day}^{-1}$ ($44.0 \pm 0.1 \mu\text{Hz}$).

With the value of $\Delta\nu$ and the empirical relation by García Hernández et al. (2017), we can estimate the stellar mean density and the surface gravity as: $\rho = 0.22 \pm 0.02 \text{ g cm}^{-3}$ and $\log g = 3.99 \pm 0.06$.

4. Stellar Model and Fitting Results

A grid of stellar evolutionary models was constructed and their corresponding adiabatic frequencies were calculated using the Modules for Experiments in Stellar Astrophysics (MESA; Paxton et al. 2011, 2013, 2015, 2018, 2019) and the stellar oscillation code GYRE (Townsend & Teitler 2013). The construction of our theoretical models are based on the OPAL opacity table GS98 (Grevesse & Sauval 1998) series. In the convective region the classical mixing length theory (Böhm-Vitense 1958), with mixing-length parameter $\alpha = 1.90$ (Paxton et al. 2013), was used. Effects of element diffusion, convective overshooting, and rotation are not included in our calculations.

In our calculations, we set the initial helium fraction $Y = 0.249 + 1.33Z$ (Li et al. 2018) as a function of the metallicity Z . We chose to survey a range of models with different metallicities between $0.002 \leq Z \leq 0.032$ in steps of 0.002, and determine the best-fitting mass and age. The stellar mass M varies from 1.50 to $2.80 M_{\odot}$ with a step of $0.01 M_{\odot}$. Each model in the above grid was evolved from the zero-age MS to the post-MS stage with $T_{\text{eff}} = 5600 \text{ K}$.

Due to the high quality of the TESS data, the two dominant pulsation mode frequencies and their frequency ratio are very precise. For further confirmation we also calculated the absolute magnitudes for TIC 448892817 using

$$M_V = V - 5 \log d + 5 - A_V, \quad (2)$$

where M_V and V denote the absolute and apparent magnitudes in the V band, respectively, A_V is the extinction due to interstellar dust, and d is the distance in pc. Extinctions were derived from Schlafly & Finkbeiner (2011). The distance we use is obtained from Bailer-Jones et al. (2021). According to

the apparent magnitudes V ($12.659 \pm 0.114 \text{ mag}$) given by Stassun et al. (2019), the M_V was obtained as $2.11^{+0.01}_{-0.02} \text{ mag}$, which is consistent with the P-L relation obtained by Ziaali et al. (2019).

The frequency and frequency ratio of radial modes depend primarily on the mass, age, evolutionary stage, and metallicity. Then a sensible method to model TIC 448892817 is by using Petersen diagrams. Petersen diagrams, therefore, provides a useful diagnostic method in terms of constraining these parameters of radial pulsators (e.g., Petersen 1973; Petersen & Christensen-Dalsgaard 1996; Daszyńska-Daszkiewicz et al. 2020; Bowman et al. 2021; Lv et al. 2022). We provide the best-fitting mass, Z , effective temperature, luminosity, surface gravity, age, theoretical frequency of fundamental, first overtone radial modes, and their ratios listed in Table 4. The ratio f_1/f_2 is mostly in the narrow range $0.77 < P_1/P_0 < 0.78$. Lower metallicity has the effect of shifting period ratios toward slightly higher values for the same mass (Balona et al. 2012). As can be seen from the table, the model ratios are closer to the observed values for models with lower metal abundances. These models with low metallicity give temperatures that are significantly larger than the typical temperature range of δ Scuti stars and the observed values from LAMOST (Cui et al. 2012). Moreover, the metallicity obtained from LAMOST was also significantly greater than 0.001. In Figure 4 we showed the evolutionary tracks of the models in Table 3 except for the low-metallicity models from the zero-age MS to the post-MS stage in order to better understand the evolution of TIC 448892817. The color lines represent different combinations of metallicity Z and mass M . Then, by using the method from Chen et al. (2019) to select the best-fitting models, the goodness of fit can be obtained, by comparing model frequencies with the observed frequencies F_0, F_1 . In order to be in line with the derived value of T_{eff} given by TESS (7253 K) and LAMOST low-resolution spectrum ($7798 \pm 200 \text{ K}$; Xiang et al. 2015), models with a broader range of temperature between 7000 and 8500 K were adopted. We note all these models suggest that TIC 448892817 is located on the close to the first turnoff of the main sequence.

Table 4

The Parameters of the Models that Reproduce Exactly the Observed Dominant Frequency f_1 as the Radial Fundamental Mode ($l = 0$) and Closely Match the Observed Frequency f_2 as the Radial First Overtone ($l = 0$)

$M (M_{\odot})$	Z	$\log T_{\text{eff}}$	$\log(L/L_{\odot})$	$\log g$	Age (10^9 yr)	f_1 (day^{-1})	f_2 (day^{-1})	f_1/f_2
1.63	0.0009	3.9865	1.5371	4.0124	1.0675	13.4376	17.2691	0.7781
1.64	0.0009	3.9882	1.5456	4.0135	1.0467	13.4378	17.2699	0.7781
1.67	0.001	3.9906	1.5604	4.0163	0.9905	13.4286	17.2652	0.7778
1.63	0.006	3.8987	1.1780	4.0203	1.1690	13.4104	17.2866	0.7758
1.65	0.006	3.9007	1.1894	4.0221	1.1083	13.4086	17.2778	0.7761
1.67	0.006	3.9107	1.2333	4.0236	1.1081	13.4111	17.2905	0.7756
1.68	0.006	3.9064	1.2177	4.0246	1.0437	13.4063	17.2755	0.7760
1.74	0.006	3.9183	1.2752	4.0299	0.9328	13.4104	17.2769	0.7762

Note. All models have an initial hydrogen abundance of $X_0 = 0.70$, mixing length parameter $\alpha = 1.9$. The mass, Z , effective temperature, luminosity, surface gravity, age, theoretical frequency of fundamental, first overtone radial modes, and their ratios of best-fitting models are provided.

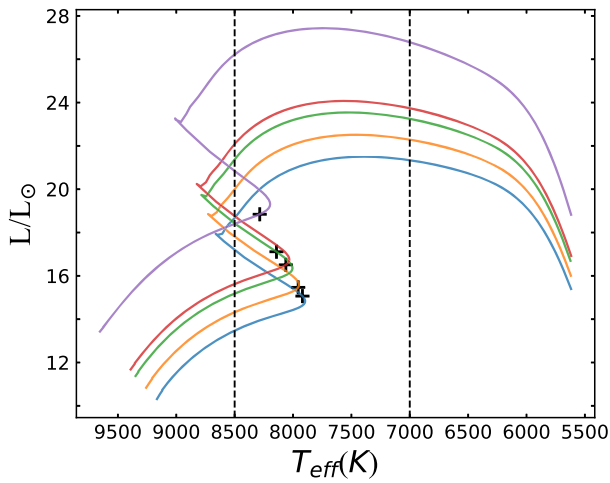


Figure 4. Evolutionary tracks from the zero-age MS to the post-MS for the 5 candidate models except for the low metallicity models, as listed in Table 3. The plus sign mark the minimum χ^2 for each specific model by fitting the calculated f_1 and f_2 with the observed values. The two vertical dotted lines mark T_{eff} at 7000 K and 8500 K, respectively.

5. Discussion and Conclusions

The models in Table 4 except for the low-metallicity models shows that the frequency ratios f_1/f_2 obtained by the models are smaller than those obtained by observation. HADS typically has a low rotational velocities with $v \sin i < 30 \text{ km s}^{-1}$, Suárez et al. (2007) propose that the effect of near degeneracy on the frequencies becomes very important for rotational velocities larger than about $15\text{--}20 \text{ km s}^{-1}$. Calculating the period ratios for different rotational velocities (rotational Petersen diagrams) and metallicities and then comparing them with classical nonrotating ones, Suárez et al. (2006), Daszyńska-Daszkiewicz et al. (2020) concludes that the period ratio f_1/f_2 increases with the increase in rotational velocity. Even for slow rotators, the effect of rotation on the period ratio can be significant (Suárez et al. 2007). Thus, if the observed ratio is larger than the calculated this might be caused by the rotation of the star.

The degeneracy between mass and age cannot generally be broken by fitting the two pulsation modes alone (Bowman et al. 2021). Hence one needs additional information, such as fitting a third mode or including spectroscopic constraints, to constrain the age of a star. The target is an excellent object of study since it has not only two confirmed radial modes but also the large separation in the low-order regime, allowing us to obtain asteroseismic indices. The models result we obtained

could be verified by comparing the stellar density deduced from the asteroseismic indices and obtained from the best-fitting models.

Hasanzadeh et al. (2021) investigate the relationship between the asteroseismic indices and the physical quantities of 438 δ Scuti stars observed by the TESS mission at 26 sectors. They used an empirical relation and a 2D autocorrelation method (see Figure 5 in Hasanzadeh et al. 2021) to derive the asteroseismic indices of these stars. Table 5 shows the parameters from Hasanzadeh et al. (2021) and the parameters obtained by our best-fitting model for TIC 448892817. We obtain essentially the same parameters as shown in the results. In addition, the basic parameters we obtained from the best-fitting model are close to the spectroscopically measured values from LAMOST. Hasanzadeh et al. (2021) gives the asteroseismic indices ν_{max} and $\Delta\nu$ for TIC 448892817 as 35.42 day^{-1} and 3.85 day^{-1} , respectively. Then using the relationship between $\Delta\nu$ and $\sqrt{\bar{\rho}}$ (Hasanzadeh et al. 2021), we derive a mean density that is basically consistent with the density obtained by our models $\rho = 0.262 \text{ g cm}^{-3}$.

To better understand the evolutionary state of this star, a comparison was made with five other HADS stars (Xue et al. 2018). According to the basic pulsation relation $P\sqrt{\bar{\rho}/\rho_{\odot}} = Q$. Since TIC 448892817 has the shortest period, according to the period density relation, the star has the largest $\bar{\rho}$ among the six HADS, revealing that TIC 448892817 is still at an earlier stage than the others, which is consistent with the tendency derived by Xue et al. (2018). This indicates that TIC 448892817 is close to entering the first turnoff of the main sequence. Although we have compared our model results with the stellar parameters calculated by the asteroseismic indices and the results are generally consistent, we still suggest high-resolution spectra is highly desired in the future, which would provide other parameters as rotational velocity, and further narrow down the parameter space of this star. In fact, an interesting result of this study is that, as suggested by Suárez et al. (2007), even a moderate rotational velocity cannot be neglected (as it is usually done) to properly model the HADS stars. The GALAH Survey (Buder et al. 2018) provides a rotational velocity for this target of $v \sin i = 12 \text{ km s}^{-1}$. Therefore, this target deserve a further study introducing pulsation models that take into account high-order effects of rotation, such as Suárez & Goupil (2008). This important result point, for the first time, to the necessity to include rotational effects to model properly HADS stars.

Table 5
Stellar Parameters Derived from Hasanzadeh et al. (2021) and the Best-fitting Model in this Work

	Mass (M_{\odot})	Radius (R_{\odot})	$\log g$	$\log(L/L_{\odot})$
Hasanzadeh et al. (2021)	1.63 ± 0.27	2.22 ± 0.15	3.96 ± 0.1	1.091 ± 0.181
This work	1.68	2.08	4.02	1.218

We thank the anonymous referee for the suggestive comments, which improved the manuscript. We would like to thank the TESS science team for providing such excellent data. J.P.G. acknowledges funding support from Spanish public funds for research from project PID2019-107061GB-C63 from the “Programas Estatales de Generación de Conocimiento y Fortalecimiento Científico y Tecnológico del Sistema de I+D+i y de I+D+i Orientada a los Retos de la Sociedad”, and from the State Agency for Research through the “Center of Excellence Severo Ochoa” award to the Instituto de Astrofísica de Andalucía (SEV-2017-0709), all from the Spanish Ministry of Science, Innovation and Universities (MCIU). A.G.H. acknowledges support from “FEDER/Junta de Andalucía-Consejería de Economía y Conocimiento” under project E-FQM-041-UGR18 by Universidad de Granada. The Large Sky Area Multi-Object Fiber Spectroscopic Telescope (LAMOST) is a National Major Scientific Project built by the Chinese Academy of Sciences. Funding for the project has been provided by the National Development and Reform Commission. LAMOST is operated and managed by the National Astronomical Observatories, Chinese Academy of Sciences.

Inlists used for our MESA analysis are available on Zenodo, at this [link](#).

ORCID iDs

Chenglong Lv <https://orcid.org/0000-0001-6354-1646>
 Ali Esamdin <https://orcid.org/0000-0003-1845-4900>
 J. Pascual-Granado <https://orcid.org/0000-0003-0139-6951>
 A. García Hernández <https://orcid.org/0000-0002-6906-4526>
 A. Hasanzadeh <https://orcid.org/0000-0002-7286-1438>

References

- Aerts, C. 2021, *RvMP*, **93**, 015001
 Aerts, C., Christensen-Dalsgaard, J., & Kurtz, D. W. 2010, *Asteroseismology* (Berlin: Springer)
 Antonello, E., & Pastori, L. 1981, *PASP*, **93**, 237
 Auvergne, M., Bodin, P., Boisnard, L., et al. 2009, *A&A*, **506**, 411
 Bailer-Jones, C. A. L., Rybizki, J., Foesneau, M., Demleitner, M., & Andrae, R. 2021, *AJ*, **161**, 147
 Balona, L. A., Lenz, P., Antoci, V., et al. 2012, *MNRAS*, **419**, 3028
 Bedding, T. R., Murphy, S. J., Hey, D. R., et al. 2020, *Natur*, **581**, 147
 Böhm-Vitense, E. 1958, *ZAp*, **46**, 108
 Bowman, D. M., Hermans, J., Daszyńska-Daszkiewicz, J., et al. 2021, *MNRAS*, **504**, 4039
 Bowman, D. M., Kurtz, D. W., Breger, M., Murphy, S. J., & Holdsworth, D. L. 2016, *MNRAS*, **460**, 1970
 Breger, M. 2000, *Delta Scuti and Related Stars*, **210**, 3
 Breger, M., Handler, G., Garrido, R., et al. 1999, *A&A*, **349**, 225
 Breger, M., Stich, J., Garrido, R., et al. 1993, *A&A*, **271**, 482
 Brown, T. M., & Gilliland, R. L. 1994, *ARA&A*, **32**, 37
 Buder, S., Asplund, M., Duong, L., et al. 2018, *MNRAS*, **478**, 4513
 Campante, T. L., Schofield, M., Kuszewicz, J. S., et al. 2016, *ApJ*, **830**, 138
 Catelan, M., & Smith, H. A. 2015, *Pulsating Stars* (New York: Wiley)
 Chen, X., Li, Y., & Zhang, X. 2019, *ApJ*, **887**, 253
 Cui, X.-Q., Zhao, Y.-H., Chu, Y.-Q., et al. 2012, *RAA*, **12**, 1197
 Daszyńska-Daszkiewicz, J., Pamyatnykh, A. A., Walczak, P., & Szweczek, W. 2020, *MNRAS*, **499**, 3034
 Daszyńska-Daszkiewicz, J., Walczak, P., Pamyatnykh, A. A., & Szweczek, W. 2022, *MNRAS*, **512**, 3551
 Dupret, M.-A., Thoul, A., Scuflaire, R., et al. 2004, *A&A*, **415**, 251
 García Hernández, A., Martín-Ruiz, S., Monteiro, M. J. P. F. G., et al. 2015, *ApJL*, **811**, L29
 García Hernández, A., Moya, A., Michel, E., et al. 2009, *A&A*, **506**, 79
 García Hernández, A., Moya, A., Michel, E., et al. 2013, *A&A*, **559**, A63
 García Hernández, A., Suárez, J. C., Moya, A., et al. 2017, *MNRAS*, **471**, L140
 García, R. A., & Ballot, J. 2019, *LRRSP*, **16**, 4
 Gilliland, R. L., Brown, T. M., Christensen-Dalsgaard, J., et al. 2010, *PASP*, **122**, 131
 Grevesse, N., & Sauval, A. J. 1998, *SSRv*, **85**, 161
 Guo, Z., Fuller, J., Shporer, A., et al. 2019, *ApJ*, **885**, 46
 Handler, G., & Breger, M. 1997, *DSSN*, **11**, 10
 Hasanzadeh, A., Safari, H., & Ghasemi, H. 2021, *MNRAS*, **505**, 1476
 Huber, D., Chaplin, W. J., Chontos, A., et al. 2019, *AJ*, **157**, 245
 Khruslov, A. V., & Kusakin, A. V. 2013, *PZ*, **33**, 6
 Koch, D. G., Borucki, W. J., Basri, G., et al. 2010, *ApJL*, **713**, L79
 Kurtz, D. W., Shibahashi, H., Murphy, S. J., Bedding, T. R., & Bowman, D. M. 2015, *MNRAS*, **450**, 3015
 Lares-Martiz, M., Garrido, R., & Pascual-Granado, J. 2020, *MNRAS*, **498**, 1194
 Lenz, P., & Breger, M. 2005, *CoAst*, **146**, 53
 Li, T., Bedding, T. R., Huber, D., et al. 2018, *MNRAS*, **475**, 981
 Loumos, G. L., & Deeming, T. J. 1978, *Ap&SS*, **56**, 285
 Lv, C., Esamdin, A., Pascual-Granado, J., Yang, T., & Shen, D. 2022, *ApJ*, **932**, 42
 Lv, C., Esamdin, A., Zeng, X., et al. 2021, *AJ*, **162**, 48
 Lv, C.-L., Esamdin, A., Liu, J.-H., Zeng, X.-Y., & Yang, T.-Z. 2021, *RAA*, **21**, 224
 McNamara, D. H. 2000, in *ASP Conf. Ser. 210, Delta Scuti and Related Stars*, ed. M. Breger & M. H. Montgomery (San Francisco, CA: ASP), 373
 Miszuda, A., Szweczek, W., & Daszyńska-Daszkiewicz, J. 2021, *MNRAS*, **505**, 3206
 Mombarg, J. S. G., Van Reeth, T., & Aerts, C. 2021, *A&A*, **650**, A58
 Montgomery, M. H., & O’donoghue, D. 1999, *DSSN*, **13**, 28
 Murphy, S. J., Bedding, T. R., Niemczura, E., Kurtz, D. W., & Smalley, B. 2015, *MNRAS*, **447**, 3948
 Murphy, S. J., Saio, H., Takada-Hidai, M., et al. 2020, *MNRAS*, **498**, 4272
 Niu, J.-S., Fu, J.-N., Li, Y., et al. 2017, *MNRAS*, **467**, 3122
 Ouazzani, R.-M., Roxburgh, I. W., & Dupret, M.-A. 2015, *A&A*, **579**, A116
 Páparó, M., Benkő, J. M., Hareter, M., & Guzik, J. A. 2016, *ApJS*, **224**, 41
 Paxton, B., Bildsten, L., Dotter, A., et al. 2011, *ApJS*, **192**, 3
 Paxton, B., Cantiello, M., Arras, P., et al. 2013, *ApJS*, **208**, 4
 Paxton, B., Marchant, P., Schwab, J., et al. 2015, *ApJS*, **220**, 15
 Paxton, B., Schwab, J., Bauer, E. B., et al. 2018, *ApJS*, **234**, 34
 Paxton, B., Smolec, R., Schwab, J., et al. 2019, *ApJS*, **243**, 10
 Petersen, J. O. 1973, *A&A*, **27**, 89
 Petersen, J. O., & Christensen-Dalsgaard, J. 1996, *A&A*, **312**, 463
 Poretti, E., Rainer, M., Weiss, W. W., et al. 2011, *A&A*, **528**, A147
 Poretti, E., Suárez, J. C., Niarchos, P. G., et al. 2005, *A&A*, **440**, 1097
 Ramón-Ballesta, A., García Hernández, A., Suárez, J. C., et al. 2021, *MNRAS*, **505**, 6217
 Reese, D., Lignières, F., & Rieutord, M. 2008, *A&A*, **481**, 449
 Ricker, G. R., Winn, J. N., Vanderspek, R., et al. 2015, *JATIS*, **1**, 014003
 Saio, H., Kurtz, D. W., Takata, M., et al. 2015, *MNRAS*, **447**, 3264
 Schläfl, E. F., & Finkbeiner, D. P. 2011, *ApJ*, **737**, 103
 Stassun, K. G., Oelkers, R. J., Paegert, M., et al. 2019, *AJ*, **158**, 138
 Stellingwerf, R. F. 1979, *ApJ*, **227**, 935
 Stello, D., Saunders, N., Grunblatt, S., et al. 2022, *MNRAS*, **512**, 1677
 Suárez, J. C., García Hernández, A., Moya, A., et al. 2014, *A&A*, **563**, A7
 Suárez, J. C., Garrido, R., & Goupil, M. J. 2006, *A&A*, **447**, 649
 Suárez, J. C., Garrido, R., & Moya, A. 2007, *A&A*, **474**, 961
 Suárez, J. C., & Goupil, M. J. 2008, *Ap&SS*, **316**, 155
 Thomson-Paressant, K., Neiner, C., Zwintz, K., & Escorza, A. 2021, *MNRAS*, **500**, 1992

- Townsend, R. H. D., & Teitler, S. A. 2013, [MNRAS](#), **435**, 3406
- Uytterhoeven, K., Moya, A., Grigahcencu, A., et al. 2011, [A&A](#), **534**, A125
- Viskum, M., Kjeldsen, H., Bedding, T. R., et al. 1998, [A&A](#), **335**, 549
- Walker, G., Matthews, J., Kuschnig, R., et al. 2003, [PASP](#), **115**, 1023
- Xiang, M. S., Liu, X. W., Yuan, H. B., et al. 2015, [MNRAS](#), **448**, 822
- Xue, H.-F., Fu, J.-N., Fox-Machado, L., et al. 2018, [ApJ](#), **861**, 96
- Yang, T.-Z., Esamdin, A., Fu, J.-N., et al. 2018, [RAA](#), **18**, 002
- Yang, X. H., Fu, J. N., & Zha, Q. 2012, [AJ](#), **144**, 92
- Yu, J., Huber, D., Bedding, T. R., et al. 2018, [ApJS](#), **236**, 42
- Ziaali, E., Bedding, T. R., Murphy, S. J., et al. 2019, [MNRAS](#), **486**, 4348